ADVANCED MATERIALS
www.advmat.de

Crossing the Dimensional Divide with Optoelectronic Tweezers: Multicomponent Light-Driven Micromachines with Motion Transfer in Three Dimensions

Gong Li, Bingrui Xu, Xiaopu Wang, Jiangfan Yu, Yifan Zhang, Rongxin Fu, Fan Yang, Hongcheng Gu, Yuchen Huang, Yujie Chen, Yanfeng Zhang, Zhuoran Wang, Guozhen Shen, Yeliang Wang, Huikai Xie, Aaron R. Wheeler, Jiafang Li, and Shuailong Zhang**

Micromachines capable of performing diverse mechanical tasks in complex and constrained microenvironments are of great interest. Despite important milestones in this pursuit, until now, micromachines are confined to actuation within a single 2D plane due to the challenges of transferring motion across different planes in limited space. Here, a breakthrough method is presented to overcome this limitation: multi-component micromachines that facilitate 3D motion transfer across different planes. These light-driven 3D micromachines, fabricated using standard photolithography combined with direct laser writing, are assembled and actuated via programmable light patterns within an optoelectronic tweezers system. Utilizing charge-induced repulsion and dielectrophoretic levitation effects, the micromachines enable highly efficient mechanical rotation and effective inter-component motion transfer. Through this work, fascinating patterns of similarities are unveiled for the new microscale 3D systems when compared with the macro-scale world in which they live, paving the way for the development of micromechanical devices and microsystems with ever increasing functionality and versatility.

1. Introduction

Micromachines are miniature mechanical or electromechanical devices with sizes ranging from several micrometers to several millimeters.[1] These tiny machines find wide applications in fields such as medicine,[2–5] electronics,[6,7] and robotics,[8–11] where their small size allows for precise manipulation and control in constrained environments. There are micromachines can carry internal power supplies, such as chemically driven micromotors, which convert stored chemical energy into kinetic energy, enabling motion with significant applications in targeted drug delivery and assisted reproduction.[12,13] However, this propulsion is often unidirectional and irreversible, requiring supplementary driving mechanisms. Because of the small size, most micromachines

G. Li, Z. Wang, G. Shen, Y. Wang, H. Xie, S. Zhang
School of Integrated Circuits and Electronics
Beijing Institute of Technology
Beijing 100081, China
E-mail: shuailong.zhang@bit.edu.cn

B. Xu, F. Yang, S. Zhang
Beijing Advanced Innovation Center for Intelligent Robots and Systems
School of Mechatronical Engineering
Beijing Institute of Technology
Beijing 100081, China

X. Wang, J. Yu
Shenzhen Institute of Artificial Intelligence and Robotics for Society (AIRS)
Shenzhen, Guangdong 518129, China

X. Wang, J. Yu
School of Science and Engineering
The Chinese University of Hong Kong
Shenzhen 518172, China

Y. Zhang, Y. Huang
Key Laboratory of Photochemistry
CAS Research/Education Center for Excellence in Molecular Sciences
Institute of Chemistry
Chinese Academy of Sciences
Beijing 100190, China

R. Fu
School of Medical Technology
Beijing Institute of Technology
Beijing 100081, China

R. Fu, H. Xie, S. Zhang
Chongqing Institute of Microelectronics and Microsystems
Beijing Institute of Technology
Chongqing 400000, China

H. Gu
State Key Laboratory of Digital Biomedical Engineering
School of Biological Science and Medical Engineering
Southeast University
Nanjing 210096, China

The ORCID identification number(s) for the author(s) of this article can be found under https://doi.org/10.1002/adma.202417742

DOI: 10.1002/adma.202417742

are powered by external physical fields, such as magnetic,[14–19] acoustic,[20–25] electric,[26–29] or optic fields.[30–35] Among these examples, light-driven micromachines represent a focal area of research, benefitting from the versatile array of optical tools that can be used to control and manipulate mechanical systems in the microscale. The most common optical technique used to control micromachines is optical tweezers (OT), which relies on the light–matter interactions and the transfer of photonic momentum.[36–40] For example, OT-driven micromachines have been used for many useful applications such as hydrodynamic manipulation,[41,42] directed tissue growth,[43] surface morphology scanning,[44,45] bio-sensing,[46] imaging[47] and precise cell/particle translation.[48–50]

Optoelectronic tweezers (OET)[51–55] has recently emerged as an alternate approach to control the behavior of microrobots and micromachines.[56–60] Compared to OT, OET offers the advantage of exerting stronger manipulation forces and is particularly well-suited for the parallel control of multiple targets simultaneously.[51–54] This capability enables the assembly and actuation of micromachines for applications in micromanipulation, microfluidics, and cell biology studies.[56–59] More importantly, the unique capabilities offer researchers the capacity to control complex micromachines that feature multiple components working together to implement sophisticated, multi-axis mechanical operations.[56–58] Despite the intriguing potential of these systems, until now, they have been confined to two dimensions (2D) and coplanar movements due to the challenges in cross-plane motion transfer, which limits their mechanical versatility and potential applications in the realistic 3D world.

Here, we introduce a method to bridge the dimensional divide: multi-component micromachines capable of inter-component motion transfer in 3D and across different planes, as depicted in **Figure 1**. Optically controlled rotatable systems have significant applications, such as altering the fluid environment around micromachines.[61] However, to achieve a more pronounced effect, larger micromechanical structures, such as those with diameters exceeding 100 micrometers, would be required, which would be challenging to manipulate using OT. Specifically, utilizing horizontally rotating and vertically rolling cogwheel microgears, both driven by OET (Figure 1A), and inspired by their macroscopic counterparts (Figure 1B), we propose and build a novel type of 3D micro-gear train system with intersecting axes (Figure 1C). This 3D assembly is achieved by using OET to position an upright cogwheel onto a custom micro-support structure fabricated via two-photon polymerization (2PP), which is then actuated by a micro-gear rotating in the XY plane. Programmable light patterns that match the layout of the micro-gear are used to operate the 3D micro-gear train system, where charge-induced repulsion and dielectrophoresis (DEP)-induced levitation are pivotal in facilitating smooth 3D manipulation and cross-plane rotational motion transfer (Figure 1C). This demonstration reveals compelling similarities in motion transfer mechanisms between microscale 3D systems and their larger macro-scale counterparts, which may unlock important new modes of advanced micro-control for applications in microfluidics, micro-electromechanical systems (MEMS), micro-robotics, and beyond.

2. Results

2.1. Micro-Gear's Flipping Behavior Controlled by OET

The unit component of the OET-actuated micromachines is a micro-gear with eight teeth arranged symmetrically around a disc with a hole in the center, as shown in **Figure 2**A,B. The micro-gear has a diameter of 200 µm and a thickness of 30 µm, as detailed in Figure S1 and Note S1 (Supporting Information). The micro-gear can be made to rotate by a rotating light pattern, which consists of an optical axle and an optical ring spanner with teeth designed to interface with those of the micro-gear (Figure 2A; Movie S1, Supporting Information). The rotating capability of the micro-gear is a key property that is leveraged to build the micromachines described below. When a solid circular light pattern is projected onto the OET bottom plate (Figure 2A), a circular virtual electrode is formed, which exerts horizontal DEP force on the micro-gear. Since the micro-gear is subjected to negative DEP force, it will be repelled by the circular light pattern and bounce off. However, when the circular light pattern keeps pushing the bounced micro-gear (Movie S2, Supporting Information), it will be flipped at some point so that the working plane of the micro-gear transforms from the horizontal plane to the vertical plane, as shown in Figure 2B. This is because the DEP force generated by the virtual electrodes not only repels the micro-gear in the horizontal plane, but also lifts the micro-gear in the vertical direction (details of which can be found in our subsequent discussion on micro-gear's lifting mechanism). After being flipped up, the micro-gear can maintain the upright standing state due to electric polarization effect. When a hollow rectangular-shaped light pattern is projected onto the flipped micro-gear (Figure 2C), it produces DEP force that traps the micro-gear in the central area, preventing the micro-gear from tipping sideways. When the light pattern moves and the flipped micro-gear is slightly displaced related to the center of the light pattern, the negative DEP force pushes the micro-gear to move forward and rotate in the vertical plane, like a rolling wheel (Figure 2C; Movie S3, Supporting Information). These results demonstrate that the flipped micro-gear can rotate in the vertical plane when subjected to DEP manipulation force.

Y. Chen, Y. Zhang
State Key Laboratory of Optoelectronic Materials and Technologies
School of Electronics and Information Technology
Sun Yat-Sen University
Guangzhou 510275, China
A. R. Wheeler
Institute of Biomedical Engineering
University of Toronto
Toronto, ON M5S 3E1, Canada
A. R. Wheeler
Department of Chemistry
University of Toronto
Toronto, ON M5S 3H6, Canada
A. R. Wheeler
Donnelly Centre for Cellular and Biomolecular Research
University of Toronto
Toronto, ON M5S 3E1, Canada
J. Li
School of Physics
Beijing Institute of Technology
Beijing 100081, China
E-mail: jiafangli@bit.edu.cn

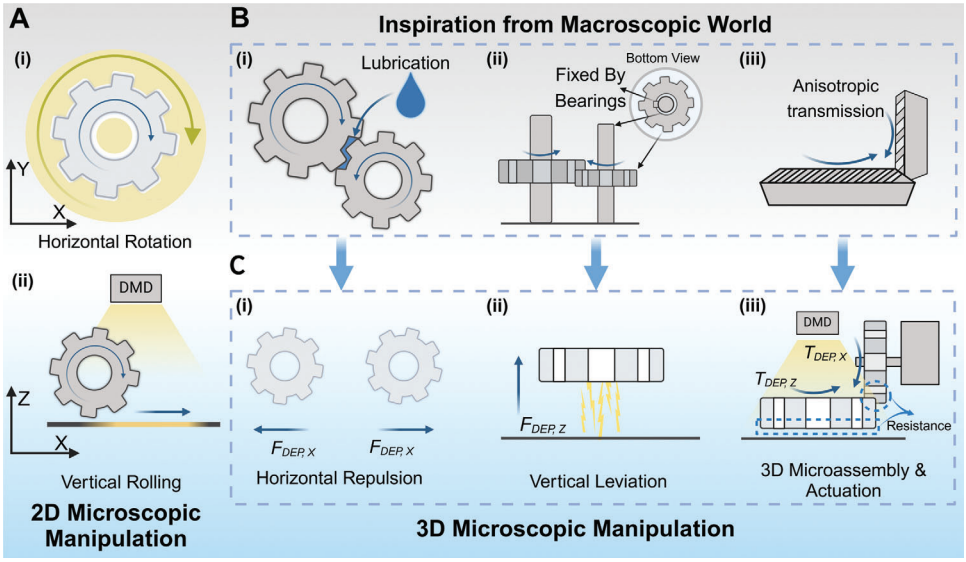

Figure 1. Building multi-component micromachines that can operate across three dimensions. A) 2D microscopic manipulation of cogwheel micro-gears, including i) horizontal rotation in the XY-plane and ii) vertical rolling in the ZX-plane. B) Gears in the macroscopic world: i) Lubrication is commonly used to reduce friction between gears. ii) Gears are typically elevated using physical bearings to minimize friction with solid surfaces. iii) Intersecting-axis gear trains can be constructed, enabling anisotropic torque transmission. C) OET-driven micro-gears in the microscopic world: i) Surface-charge-induced horizontal repulsion within the microsystem provides an analogous effect to lubrication in the macroscopic world. ii) DEP-induced vertical levitation within the microsystem mimics the function of physical bearings in the macroscopic world. iii) Intersecting-axis micro-gear trains can be formed, offering similar capabilities to their macroscopic counterparts.

To explore the flipping behavior of micro-gears, we built two simulation models corresponding to two micro-gears with thicknesses of 30 and 60 µm, respectively (Figure S2A,B, Supporting Information). Details of the simulation model are presented in the Materials and Methods Section. The electric field distributions for micro-gears of differing thicknesses are illustrated in Figure S2C,D (Supporting Information). Notably, when a micro-gear is positioned at the edge of the circular light pattern (x = 196 µm), the relative distribution of electric field strength across the micro-gear (in the XY plane) is uneven. Particularly, the field strength is much stronger on the right side of the micro-gear (see Figure 2D). Consequently, a repulsive DEP force is exerted on the micro-gear in the XY plane, with the resultant force directed toward the right (positively along the X-axis and away from the light pattern), verifying the observations from the experiment (Movie S2, Supporting Information). Notably, the variation in relative electric field strength for the 30-µm-thick micro-gear is more pronounced than that for the 60-µm-thick micro-gear, thereby rendering the DEP repulsive force considerably stronger for the thinner micro-gear. Similarly, the distributions of relative electric field strength across the micro-gears in the XZ plane (see Figure 2E) suggest that the thinner micro-gear also experiences a stronger vertical DEP force. Finally, the DEP torque responsible for flipping the micro-gear was computed and depicted in Figure 2F. It was observed that the DEP torque exerted on micro-gears of different sizes exhibits no significant difference in absolute value. However, owing to variations in thickness/structure-induced rotational inertia, a notable difference exists in the DEP angular acceleration for micro-gears of different sizes, as illustrated in Figure 2G. These findings suggest that the 30-µm-thick micro-gear is more easily to flip in the OET system compared to the 60-µm-thick micro-gear and is therefore chosen for constructing the multi-component micromachines capable of operating in 3D, as reported in the following.

Utilizing a circular light pattern to push the micro-gear and induce its flipping typically requires extensive motion over a long range and a sizable working space. However, in the context of OET devices, space is often limited, emphasizing the significance of achieving micro-gear flipping within its original position or within a confined area. Illustrated in **Figure 3A** are the schematic and experimental images demonstrating the use of a specially designed rectangular-shaped light pattern to achieve micro-gear flipping in its original position. When the micro-gear is positioned to the right side of the light pattern, it will be propelled to the left by the OET and initiate flipping as it approaches the center of the light pattern. The direction and angular velocity of the flip can be precisely controlled by adjusting the relative distance between the micro-gear and the center of the light pattern, as depicted in Figure 3B,C (further details provided in Movie S4, Supporting Information). It is observed that the flipping angular velocity of the micro-gear increases with the relative distance to the center of the light pattern. Nevertheless, due to the constraints imposed by the light pattern, when the micro-gear is positioned too far from the center of the light pattern (exceeding 70 µm), it will experience horizontal repulsion from the light pattern, posing challenges to the flipping process. To analyze the distribution of DEP force acting on the micro-gear, simulations were conducted with details described in the Materials and Methods section. Figure 3D illustrates the simulated DEP flipping angular acceleration of the micro-gear at different relative positions to the center of the light pattern. Additionally, Figure 3E depicts the simulated DEP horizontal acceleration (XY plane) of the micro-gear at different

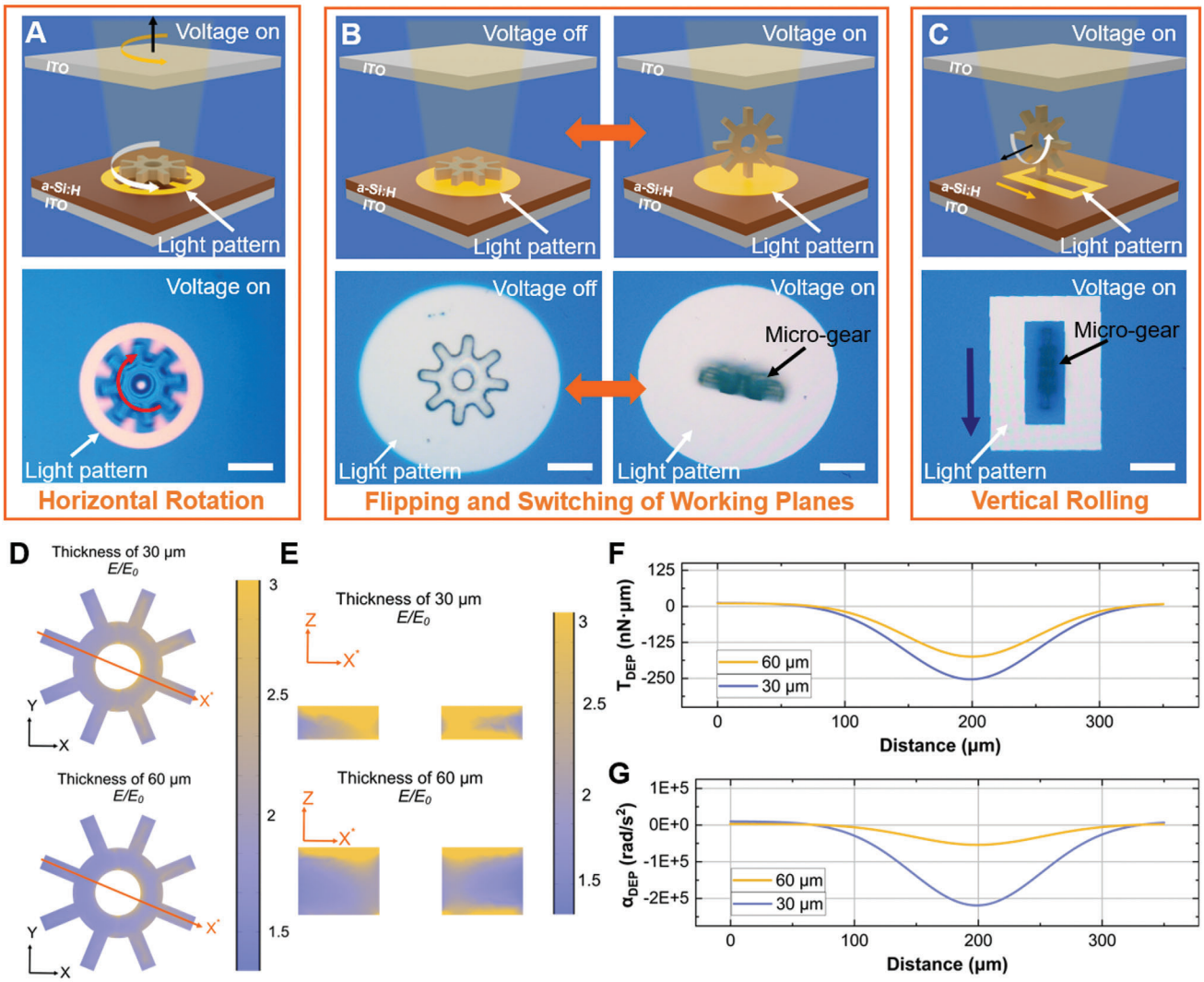

Figure 2. Flipping behavior of the micro-gear. A) Schematic diagram and microscope image of a micro-gear rotating in the horizontal plane (Movie S1, Supporting Information). B) Schematic diagram and microscope image of a lying micro-gear at the center of a circular light patten when the voltage is switched off. When the voltage is switched on, the micro-gear flips to become upright standing and switches the working planes. The transformation of the micro-gear from lying state to the upright standing state was achieved via pushing the micro-gear with a circular light pattern (Movie S2, Supporting Information). C) Schematic diagram and microscope image of an upright standing micro-gear being pushed by a hollow rectangular light pattern and roll forward in the vertical plane (Movie S3, Supporting Information). D) Simulated relative electric field distributions in the XY plane for the 30-μm-thick and 60-μm-thick micro-gear (E_0 = 20 V/225μm). E) Simulated relative electric field distributions in the XZ plane for the 30-μm-thick and 60-μm-thick micro-gear (E_0 = 20 V/225μm). F) Simulated DEP flipping torque for the 30-μm-thick and 60-μm-thick micro-gear at different positions relative to the center of the circular light pattern. G) Simulated flipping angular acceleration for the 30-μm-thick and 60-μm-thick micro-gear at different positions relative to the center of the circular light pattern.

relative positions to the center of the light pattern. The simulation results align closely with the experimental results presented in Figure 3C.

Shown in Figure 3F,G are the distributions of the electric potential and the relative electric field strength of a micro-gear positioned 47 μm to the right of the center of the light pattern, where it experiences the strongest DEP flipping torque. According to the simulation results, the micro-gear in this position encounters horizontal attracting DEP force, prompting its movement toward the center of the light pattern, as well as DEP flipping torque, which causes it to flip up. Furthermore, the simulation results indicate that the portion of the micro-gear closest to the center of the light pattern initiates flipping first, aligned with the experimental observations shown in Movie S4 (Supporting Information). Consequently, by adjusting the relative position of the micro-gear to the light pattern, precise control over the micro-gear's flip within a confined area were achieved. Notably, the flip axis of the micro-gear can be manipulated by adjusting the position and rotation angle of the light pattern, as demonstrated in Movie S5 (Supporting Information). These results are important as they highlight the capacity of OET-manipulated micro-gears to obtain degrees of freedom in motion, encompassing both

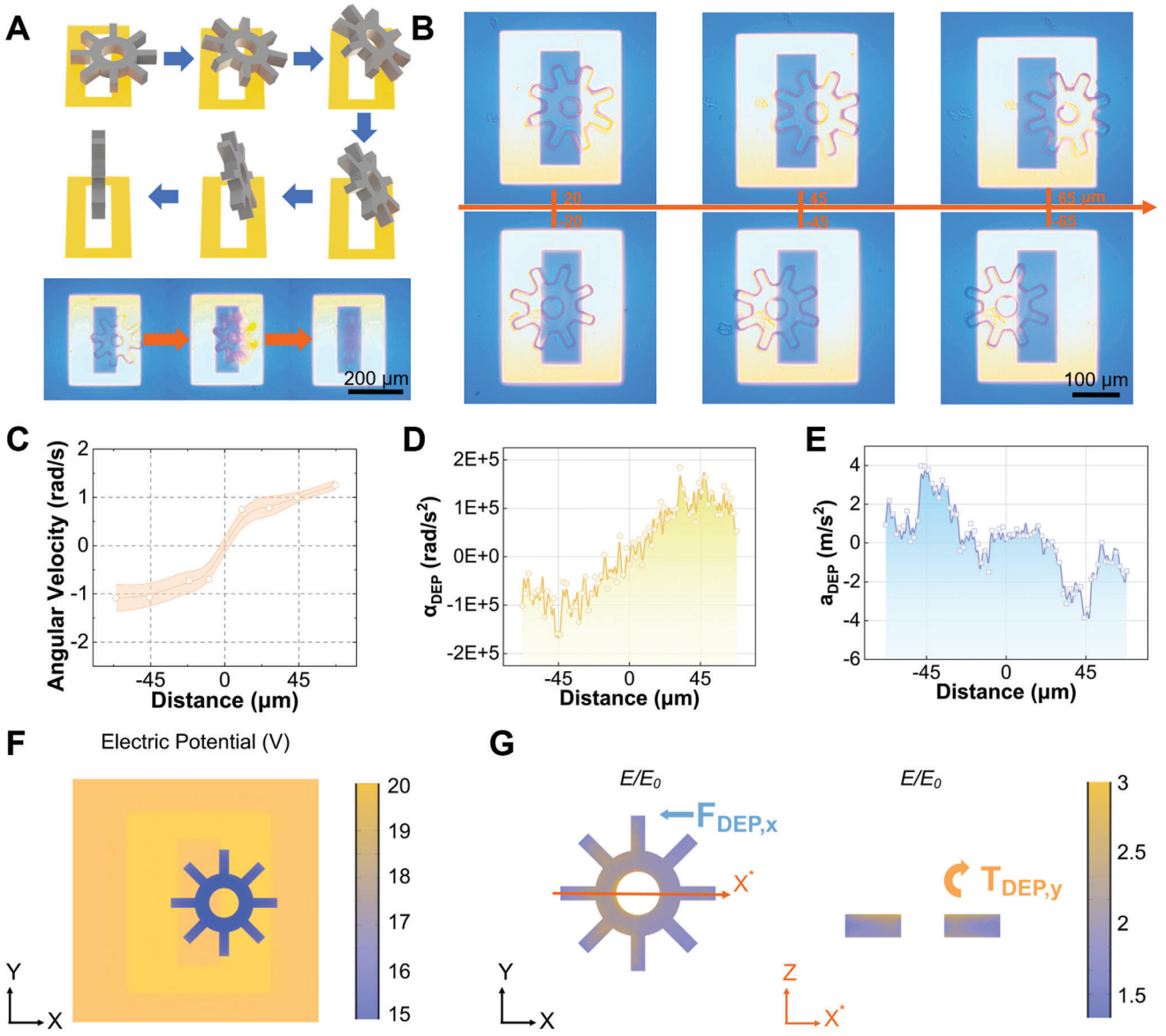

Figure 3. Controlled flip of micro-gear with OET. A) Schematic diagram and microscope images showing the flipping process of a micro-gear in a confined area. B) Microscope images and C) measured flipping angular velocity of a micro-gear with different distances to the center of the light pattern. More details provided in Movie S4 (Supporting Information). D) Simulated flipping angular acceleration and E) simulated horizontal acceleration of the micro-gear with different distances to the center of the light pattern. F) Simulated electric potential distribution and G) simulated relative electric field strength distribution of the bottom surface and XZ cross-section of the micro-gear, positioned 47 μm to the right of the light pattern center.

translation and rotation along three axes, which is important for the development of multi-component micromachines capable of motion transfer in 3D and across different planes.

2.2. Assembly and Operation of Micro-Gear train Systems

A micro-gear train is a mechanical system comprising multiple gears that collaborate to transmit power from one shaft to another. It serves as a foundational element in various mechanical systems, offering a crucial method to transmit and regulate rotational motion. In our prior research, we showcased the application of OET in constructing micro-gear trains capable of executing 2D coplanar movements.[56] Inspired by existing 3D optical manipulation technologies,[12,61,62] we fabricated micro-supports to improve the stability and controllability of 3D manipulation. In this study, we have dramatically improved on previous efforts, crossing the dimensional divide to expand the micro-gear train's capabilities to facilitate 3D movement and effective motion transfer.

Figure 4A shows the scanning electron microscope (SEM) images of the microstructures fabricated on the OET top plate, consisting of a thin micro-wall with four micro-rods on the sides. A top-view microscope image of the fabricated microstructure

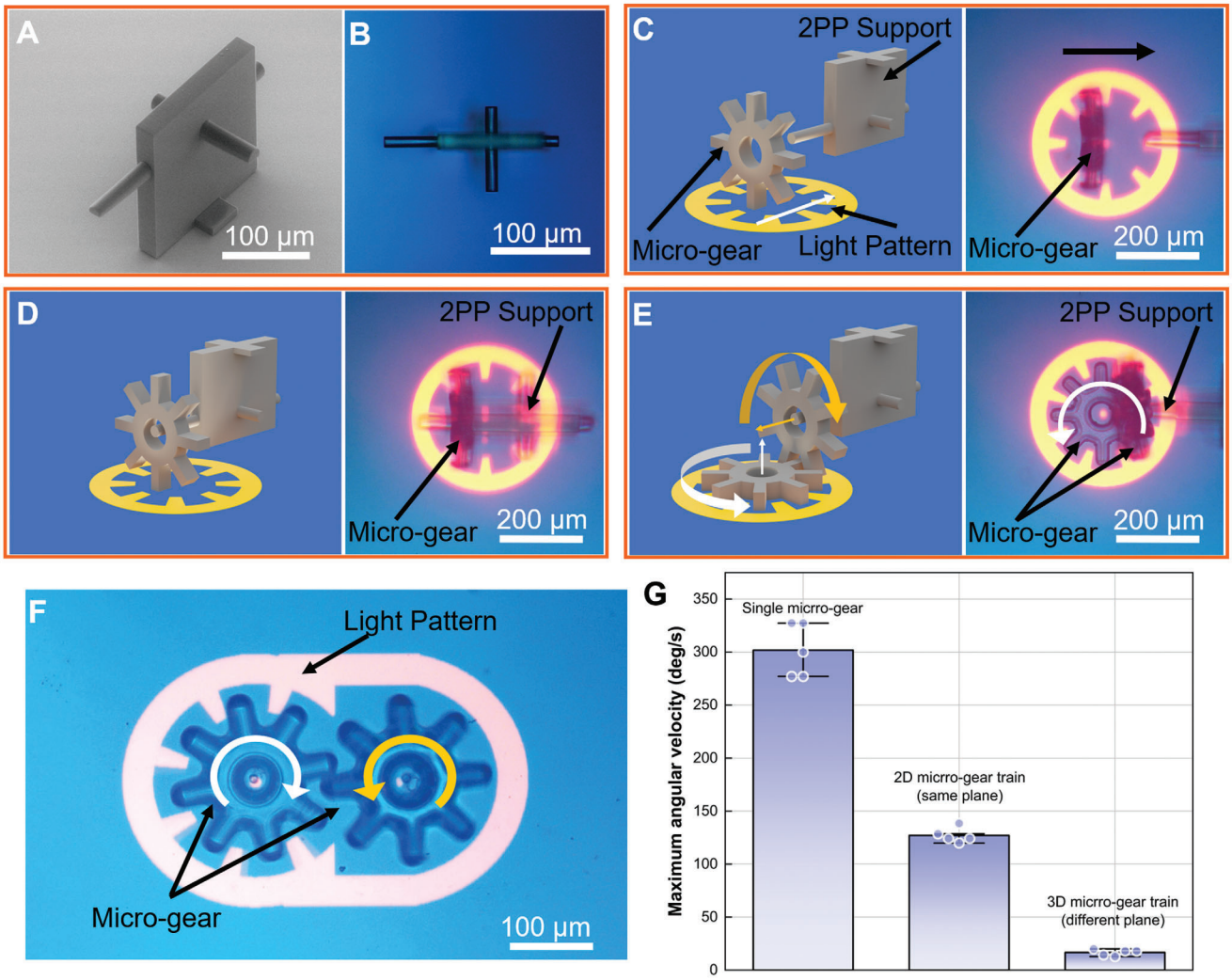

Figure 4. Assembly and operation of micro-gear trains with OET. A) SEM images of the mechanical support structure created by 2PP. B) Top-view optical microscope image of the mechanical support. C) Schematic diagram alongside an experimental microscope image demonstrating the assembly process of a flipped micro-gear with the mechanical support. D) Schematic diagram and experimental microscope image showing the interconnected structure following the assembly of the micro-gear with the mechanical support. E) Schematic diagram and experimental microscope image of a 3D cross/multi-planar micro-gear train system in operation. F) Microscope image of a 2D co-planar micro-gear train system in operation (Movie S1 (Supporting Information), Clip 2). G) The measured maximum angular velocity of a single micro-gear, a 2D micro-gear train, and a 3D micro-gear train. More details on the assembly and driving of 3D micro-gear train with OET are provided in Movie S6 (Supporting Information).

is presented in Figure 4B. This microstructure is generated using two-photon polymerization (2PP), a precision laser writing technique capable of selectively polymerizing UV-curable materials to create 3D microstructures with submicron resolution.[63–65] The 2PP-fabricated microstructure functions as a mechanical support for the flipped micro-gear, which can be manipulated by a light pattern and assembled with the 2PP support, as depicted in Figure 4C (with further details provided in Movie S6, Supporting Information).

Following assembly, a micro-rod passes through the central hole of the flipped micro-gear, establishing a stable interconnection between the micro-gear and the 2PP support, as illustrated in Figure 4D. After the assembly, a micro-gear rotating in the horizontal plane was precisely positioned to engage with the flipped micro-gear. Upon the application of torque, the flipped micro-gear started rotation in the vertical plane, as depicted in Figure 4E and Movie S6 (Supporting Information). Here, the horizontally rotating micro-gear acts as an active micromotor, propelling the flipped micro-gear and facilitating its rotation in the vertical plane, thereby enabling the microscopic transmission gear set (a micro-gear-train system) to achieve 3D cross/multi-plane motion transfer and anisotropic torque transmission. In this configuration, the micro-rod of the 2PP support plays a crucial role as it serves as the physical axis for the vertically rotating micro-gear.

In the experiment, it was observed that the angular velocity of the 3D micro-gear train is lower than that of a co-planar 2D micro-gear train system (Figure 4F; Movie S1, Supporting Information, similar to methods reported previously.[56] As illustrated in Figure 4G, the maximum angular velocity of the 3D

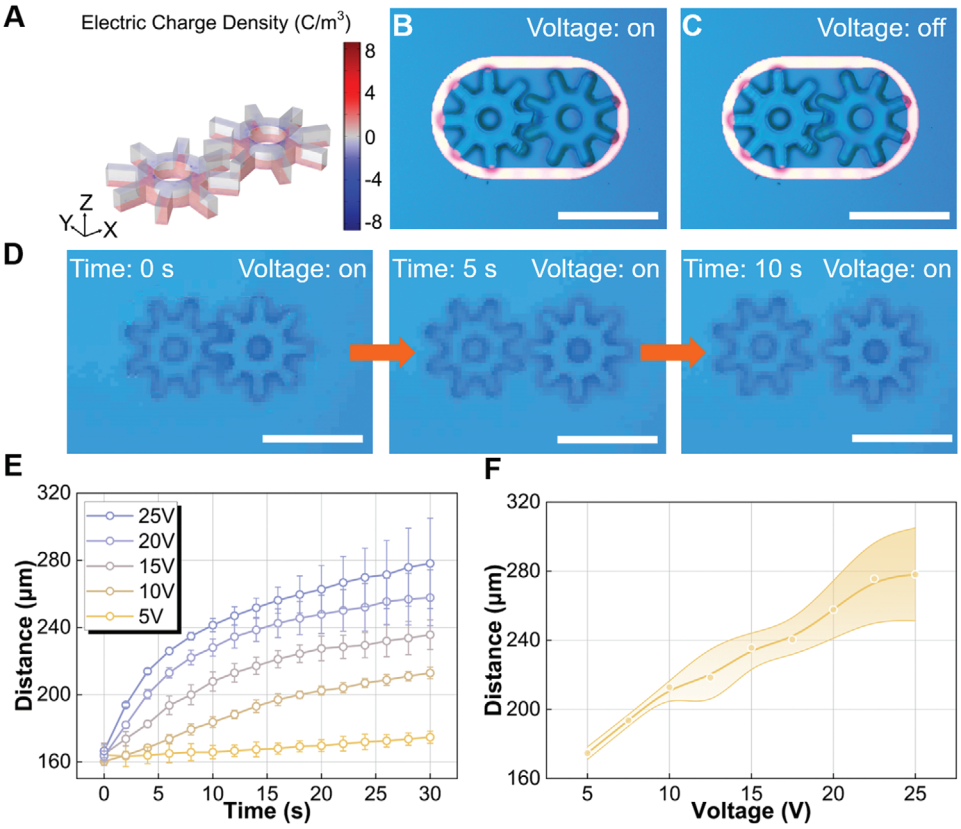

Figure 5. Repulsion mechanism of micro-gears. A) Simulated surface charge distribution in a 2D micro-gear train system. B) Microscope image illustrating the utilization of a light pattern to facilitate the physical engagement of two micro-gears. C) Microscope image demonstrating that deactivating the bias voltage while maintaining illumination has minimal impact on the motion of micro-gears. D) Microscope images depicting the physical separation of two micro-gears after deactivation of the light pattern while sustaining the voltage. E) Time-dependent measurement of the center-to-center distance between the micro-gears at various bias voltages. F) Voltage-dependent measurement of the center-to-center distance between the micro-gears subsequent to voltage activation while maintaining darkness for a duration of 30 s.

micro-gear train remains at 17 deg s^{-1}, which is less than that of the 2D micro-gear train (120 deg s^{-1}). To elucidate this phenomenon, simulations were conducted to analyze the flow field distribution around the micro-gear train, with detailed information provided in Figure S3 and Note S2 (Supporting Information). Based on the simulation results depicted in Figure S3 (Supporting Information), the mechanical efficiency of the 3D micro-gear train was calculated to be 6.46% (Figure S4A, Supporting Information). Moreover, Figure S4B (Supporting Information) demonstrates the torque distribution in the 3D micro-gear train, revealing a predominant torque allocation on the horizontally rotating micro-gear rather than the vertically rotating one. This observation suggests mechanical losses during torque transmission within the 3D micro-gear train system, possibly attributed to frictional interactions among various micro-gear components and between the flipped micro-gear and its mechanical support. In contrast, the mechanical efficiency of the 2D micro-gear train is remarkably high at 84.46%, exceeding conventional expectations for such microsystems. It is worth noting that even commonly used macro-scale gear systems, when operating without lubrication, may experience a significant drop in efficiency to 50%-70% or even lower in most cases.[66] This finding prompts a deeper investigation into the underlying physical mechanisms driving this phenomenon that will presented in the following section.

2.3. Mechanism of electric lubrication in OET-driven micro-gear train

The high mechanical efficiency observed in the OET-driven micro-gear train implies minimal friction among the micro-gears, suggestive of a lubrication-like mechanism. To investigate this phenomenon, systematic simulations were conducted to analyze the interactions among the micro-gears (simulation model provided in Figure S5A,B, Supporting Information). Illustrated in **Figure** 5A is the simulated surface charge distribution of the 2D coplanar micro-gear train system.

It was found that the surface charge distribution exhibited parity across the two micro-gears, with equivalent charge residing at the interfaces between them. Consequently, an electrostatic repulsive force manifests between the micro-gears, quantitatively determined through simulation to be 2511.8 pN under the AC bias of 20 V at 10 kHz. It is posited that this repulsive force instigates the lubrication-like phenomenon, thereby significantly mitigating physical interfacial friction between the micro-gear

teeth and increasing the mechanical efficiency and torque transmission within the micro-gear train system. Similarly, investigation of the surface charge distribution within the 3D micro-gear train system unveils a slightly diminished uniformity relative to its 2D counterpart (Figure S5C, Supporting Information), indicating a reduced repulsive force between micro-gears and potentially stronger frictional interactions.

To verify the simulation results, a series of experiments were conducted. Illustrated in Figure 5B are two micro-gears arranged in a configuration for mutual engagement. Following the cessation of voltage application while maintaining illumination, minimal displacement of the micro-gears is observed, as depicted in Figure 5C, suggesting negligible influence of the light pattern on the inter-gear physical interactions. Conversely, upon deactivating the light pattern and sustaining the voltage, rapid separation of the micro-gears occurs, as shown in Figure 5D (with additional details provided in Figure S5D and Movie S7, Supporting Information). Figure 5E depicts the temporal evolution of the center-to-center distance between the micro-gears under different applied bias (see Figure S6, Supporting Information for more measured results). Notably, the separation between the micro-gears increases over time, while the rate of change in center-to-center distance diminishes, likely attributable to the attenuation of repulsive forces as the micro-gears become more distanced. Additionally, Figure 5F illustrates the voltage-dependent center-to-center distances between the micro-gears after 30 s of voltage application. Evidently, higher voltages prompt greater separation between the micro-gears, indicative of intensified surface-charge-induced repulsive forces. These findings underscore the capability of micro-gear surface charges to generate repulsive forces, thereby mitigating physical frictions and facilitating enhanced motion transfer within the micro-gear train system.

The surface-charge-assisted lubrication-like mechanism between micro-gears plays a pivotal role in augmenting the mechanical efficiency of the micro-gear train system. However, it is not the sole contributor. Subsequent experiments unveil that the heightened mechanical efficiency of the 2D micro-gear train system also owes to the levitation phenomenon exhibited by the micro-gears, which notably diminishes friction between the micro-gears and the OET bottom plate. The levitation mechanism is elucidated in Movie S8 (Supporting Information) and **Figure 6**A, wherein the application of a bias voltage to the OET device engenders an upward lifting force on the micro-gear, causing it to ascend from the OET bottom plate by a discernible distance and traverse freely. To quantitatively assess the elevation achieved by the micro-gear, a computational methodology was devised,[67,68] as presented in Figure S7 (Supporting Information). This approach entails Z-axis scanning of the micro-gear at increments of 0.1 µm. Prior to each scan, the microscope's focal plane is adjusted to achieve optimal clarity of the micro-gear's top surface (in the absence of voltage application, with the micro-gear resting on the OET bottom plate). Subsequently, the Z-axis scan is executed, and the Z coordinates of the initial point are recorded.

To determine the uplifted height of the micro-gear post-voltage application, the starting point of the Z-axis scan is maintained consistent with its counterpart during the non-voltage condition. Illustrated in Figure 6B is the Z-axis scanning process without voltage application, characterized by a transition from clear to blurred micro-gear contours, with the micro-gear deemed absent from the image upon the algorithm's inability to distinguish it. The count of frames containing the micro-gear is then recorded. Figure 6C depicts the scanning procedure after bias voltage application, wherein the micro-gear outline gradually shifts from blurry to clear and then from clear to blur, enabling frame count determination through the same algorithm. Subsequently, the micro-gear's lift distance is computed by multiplying the Z-axis scan step size (0.1 µm) by the difference in frame numbers between the two Z-axis scans (detailed calculation method is provided in Figure S7, Supporting Information). Notably, at an AC bias of 20V at 10 kHz, the micro-gear attains a levitation height of ≈5.8 µm, as illustrated in Figure 6D.

To elucidate the levitation mechanism, a simulation model was built to explore the lifting force acting upon micro-gears of different thicknesses. As illustrated in Figure 6E,F, the presence of a micro-gear induces a more concentrated and increasingly inhomogeneous electric field distribution, thereby subjecting the micro-gear to an upward DEP force. Particularly noteworthy is the discernible impact of micro-gears on the inhomogeneity of the surrounding electric field, which is more pronounced for micro-gears with a thickness of 30 µm, indicating that thinner micro-gears experience a more robust upward DEP force compared to their thicker counterparts. The acceleration of the DEP force acting on 30-µm-thick and 60-µm-thick micro-gears is also simulated and presented in Figure 6G,H, respectively. From these simulations, it becomes evident that while resting on the OET bottom plate, the micro-gear experiences an intensified upward DEP force, prompting its elevation as observed in the experiment. As the lift distance increases, the DEP force undergoes a rapid decline until it reaches equilibrium with the viscous and gravitational forces acting to draw the micro-gear downward. At this juncture, the upward motion of the micro-gear halts, maintaining a distance from the surface of the OET bottom plate without physical contact. These observations underscore the occurrence of a DEP-assisted levitation mechanism on the micro-gear, thereby mitigating physical frictions between micro-gears and the OET bottom plate and facilitating smooth rotational motion transfer within the assembled microscopic transmission gear set.

3. Discussion

Compared to existing 3D manipulation methods,[13,61,62] we utilized the advantages of OET in precision and sufficient manipulation force, combined with micro-gears, to achieve more controllable and robust 3D motion and transmission. In this study, we presented the utilization of OET to proficiently manipulate micro-gears and micro-gear train systems, thereby substantially broadening the functional capabilities of OET from traditional 2D co-planar manipulation to intricate 3D cross/multi-planar manipulation. Employing diverse strategies, on-demand flipping of micro-gears was successfully achieved, with experimental outcomes validated through numerical simulations and systematic analysis. To establish a 3D micro-gear train system, 2PP technology was utilized to fabricate a microstructure serving as a stable physical axis for the flipped micro-gear. This pivotal advancement facilitated the assembly and effective manipulation of 3D cross/multi-planar micro-gear train systems, with the horizontally oriented gear serving as the active component and

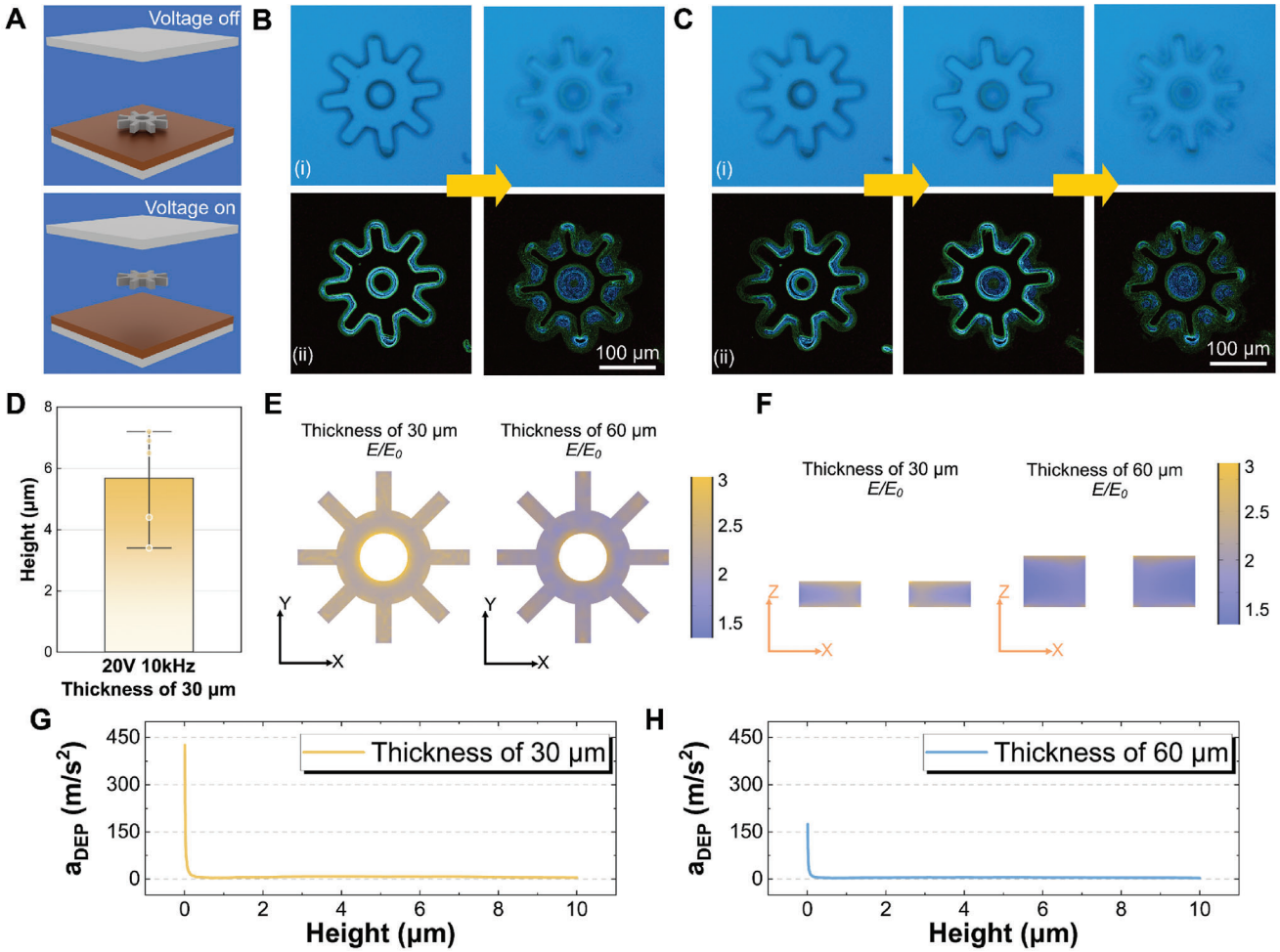

Figure 6. The levitation mechanism of micro-gear. A) Schematic diagram illustrating the lifting of a micro-gear under the influence of an electric field. B) Z-axis scan of the micro-gear without voltage applied. In i) bright-field microscope images and ii) microscope images based on SURF transformation, the contour of the micro-gear transitions from clear to blurred. C) Z-axis scan of the micro-gear after voltage activation. In i) bright-field microscope images and ii) microscope images based on SURF transformation, the contour of the micro-gear shifts from blurred to clear and then back to blurred. D) Measured lifting distance of a 30-μm-thick micro-gear at an AC bias of 20 V at 10 kHz. E) Relative electric field intensity distribution across the bottom cross-section of the 30-μm-thick micro-gear and 60-μm-thick micro-gear; F) Relative electric field intensity distribution across the longitudinal section of the 30-μm-thick micro-gear and 60-μm-thick micro-gear. G) Simulated acceleration of DEP force acting on a 30-μm-thick micro-gear at different distances to the surface of OET bottom plate. H) Simulated acceleration of DEP force acting on a 60-μm-thick micro-gear at different distances to the surface of OET bottom plate.

its flipped counterpart as the passive component. Subsequently, comprehensive experiments and systematic simulations were conducted to elucidate the smooth motion transfer within the micro-gear train system. Notably, our analysis revealed that the surface charge of the micro-gears induces repulsive forces, mitigating interfacial frictions (a phenomenon termed the surface-charge-assisted lubrication). Furthermore, we observed a remarkable DEP-induced levitation phenomenon for the micro-gears, resulting in their suspension from the surface of the OET bottom plate, thereby minimizing friction.

Such ability to engineer and control 3D micro-gear train via OET marks a significant leap forward compared to alternative light-driven microsystems and micromechanical devices. To our knowledge, this study represents a pioneering demonstration of light-driven multi-component micromachines comprising constituent units operating at distinct planes simultaneously, which may promote new applications that are currently difficult to achieve (see Figure S8, Supporting Information). Moreover particularly intriguing is the alignment between technological solutions utilized in the macroscopic world and the physical mechanisms unveiled in the microscopic realm within this study, as depicted in Figure 1B. In macroscopic micro-gear trains, for example, chemical lubricants are typically employed to mitigate physical friction between micro-gears, thereby boosting the overall mechanical efficiency. Moreover, gears are usually elevated from the base using physical bearings to reduce friction with solid surfaces. These critical technological solutions have been replicated in the micro-gear train systems driven by OET (see Figure 1C for more details). For example, the surface-charge-induced repulsive interaction between micro-gears and the DEP-induced

lifting mechanism has notably diminished physical frictions in the micro-gears comprising the micro-gear train, enabling it to exhibit exceptional mechanical performance within the OET system. Therefore, this study serves as a compelling illustration of how lessons from technical solutions and engineering principles in the macroscopic domain can inspire new ideas and methodologies for microengineering at the microscopic scale. For instance, drawing inspiration from the bevel micro-gear train systems used in the macroscopic world, we developed a corresponding 3D micro-gear train system utilizing OET technology within the micro realm, and both systems operate on similar mechanical principles. It can be envisioned that the adoption of more sophisticated fabrication techniques, such as super-resolution 2PP technique, could produce micro-gears with involute profiles and holds significant promise in substantially augmenting the performance of the 3D micro-gear train system.

In conclusion, our work demonstrates the utilization of OET in flipping, assembling, and propelling micro-gears and microscopic transmission gear sets (micro-gear trains) across both 2D and 3D configurations. We affirm that the foundational principles and mechanisms outlined in this study signify a notable progression for the microsystem field, ushering in a new era of sophisticated and applicable light-driven micromachinery capable of smooth motion transfer in 3D and across different planes. These discoveries offer potentials for enhanced manipulation capabilities and novel modes of micro-control covering a variety of applications in MEMS, microfluidics, and microrobotics, establishing the foundation for future innovations in this burgeoning domain.

Supporting Information

Supporting Information is available from the Wiley Online Library or from the author.

Acknowledgements

The authors acknowledge the technical support from the Center for Nanostructure Imaging at the Department of Chemistry, University of Toronto, the Center for Research and Applications in Fluidic Technologies (CRAFT), the Biological and Medical Engineering Core Facilities of Beijing Institute of Technology, Analysis and Testing Center of Beijing Institute of Technology. The authors also would like to thank the support from Dr Hainan Xie and Mr Wei Xie from Optoseeker Biotechnology (Shenzhen) Co., Ltd. to provide technical support to build and commercialized the OET system and Dr. Yueteng Wei for measuring the 3D profile of the micro-gear. The research was supported by the National Key R&D Program of China (Grant no. 2023YFE0112400, 2024YFC3406900, 2022YFA1207100, and 2023YFF0721500), National Natural Science Foundation of China (Grant no. 62103050, T2325005, 62375016), the Beijing Municipal Natural Science Foundation (Grant no. L246030, 4242060), the Chonqing Municipal Natural Science Foundation (Grant no. 2024NSCQ-MSX3784, 2024NSCQ-JQX0192), Shenzhen Science and Technology Program (Grant no. KJZD20240903101359020), the BIT Research and Innovation Promoting Project (Grant no. 2023CX01002), the Open Research Fund of State Key Laboratory of Digital Medical Engineering (Southeast University, Grant No. 2023-K02), Open Research Fund of Guangdong Provincial Key Laboratory of Advanced Biomaterials (Southern University of Science and Technology, Grant no. KLAB202404002), the State Key Laboratory of Optoelectronic Materials and Technologies (Sun Yat-sen University, Grant no. OEMT-2024- KF-03).

Conflict of Interest

The authors declare no conflict of interest.

Author Contributions

S.Z. conceived the idea. G.L., S.Z., Y.Z., Y.H., Z.W., G.S., and X.H. designed, fabricated, and characterized the micro-gear. G.L., S.Z., X.W., J.Y., Y.Z., and H.G. designed, fabricated, and characterized the 2PP support. G.L., B.X., and S.Z. built the simulation model and ran the simulations. G.L., S.Z., Y.Z., and Y.C. fabricated the OET device. G.L., B.X., R.F., and S.Z. carried out the experiments and analyzed the data. G.L., S.Z., B.X., F.Y., J. L., and A.R.W. prepared the figures and wrote the manuscript. All authors discussed the results and commented on the manuscript. Y.W., H.X., A.R.W, J.L., and S.Z. coordinated and supervised the project.

Data Availability Statement

The data that support the findings of this study are available from the corresponding author upon reasonable request.

Keywords

3D motion transfer, micromachine, micromanipulation, micromotor, optoelectronic tweezers, optically-induced dielectrophoresis

Received: November 15, 2024
Revised: January 23, 2025
Published online: February 13, 2025

[1] J. Liu, Z. Li, *Micromachines* **2018**, *9*, 232.
[2] Y. S. Choi, H. Jeong, R. T. Yin, R. Avila, A. Pfenniger, J. Yoo, J. Y. Lee, A. Tzavelis, Y. J. Lee, S. W. Chen, H. S. Knight, S. Kim, H.-Y. Ahn, G. Wickerson, A. Vázquez-Guardado, E. Higbee-Dempsey, B. A. Russo, M. A. Napolitano, T. J. Holleran, L. A. Razzak, A. N. Miniovich, G. Lee, B. Geist, B. Kim, S. Han, J. A. Brennan, K. Aras, S. S. Kwak, J. Kim, E. A. Waters, et al., *Science* **2022**, *376*, 1006.
[3] W. Gao, S. Emaminejad, H. Y. Y. Nyein, S. Challa, K. Chen, A. Peck, H. M. Fahad, H. Ota, H. Shiraki, D. Kiriya, D.-H. Lien, G. A. Brooks, R. W. Davis, A. Javey, *Nature* **2016**, *529*, 509.
[4] A. Zhang, E. T. Mandeville, L. Xu, C. M. Stary, E. H. Lo, C. M. Lieber, *Science* **2023**, *381*, 306.
[5] X. Cai, H. Zhang, P. Wei, Q. Liu, D. Sheng, Z. Li, B. Zhang, G. Tang, W. Zhao, Z. Ye, Z. Xue, Y. Xie, Y. Dai, C. Wang, Y. Wang, X. Fu, L. Yin, H. Peng, H. Ding, G. Zhao, X. Sheng, *Nat. Photon.* **2024**, *18*, 492.
[6] D.-H. Kim, N. Lu, R. Ma, Y.-S. Kim, R.-H. Kim, S. Wang, J. Wu, S. M. Won, H. Tao, A. Islam, K. J. Yu, T. Kim, R. Chowdhury, M. Ying, L. Xu, M. Li, H.-J. Chung, H. Keum, M. McCormick, P. Liu, Y.-W. Zhang, F. G. Omenetto, Y. Huang, T. Coleman, J. A. Rogers, *Science* **2011**, *333*, 838.
[7] B. H. Kim, K. Li, J.-T. Kim, Y. Park, H. Jang, X. Wang, Z. Xie, S. M. Won, H.-J. Yoon, G. Lee, W. J. Jang, K. H. Lee, T. S. Chung, Y. H. Jung, S. Y. Heo, Y. Lee, J. Kim, T. Cai, Y. Kim, P. Prasopsukh, Y. Yu, X. Yu, R. Avila, H. Luan, H. Song, F. Zhu, Y. Zhao, L. Chen, S. H. Han, J. Kim, et al., *Nature* **2021**, *597*, 503.
[8] M. Z. Miskin, A. J. Cortese, K. Dorsey, E. P. Esposito, M. F. Reynolds, Q. Liu, M. Cao, D. A. Muller, P. L. McEuen, I. Cohen, *Nature* **2020**, *584*, 557.
[9] Q. Liu, W. Wang, M. F. Reynolds, M. C. Cao, M. Z. Miskin, T. A. Arias, D. A. Muller, P. L. McEuen, I. Cohen, *Sci. Robot.* **2021**, *6*, eabe6663.

[10] B. J. Nelson, S. Pané, *Science* **2023**, *382*, 1120.
[11] M. Han, X. Guo, X. Chen, C. Liang, H. Zhao, Q. Zhang, W. Bai, F. Zhang, H. Wei, C. Wu, Q. Cui, S. Yao, B. Sun, Y. Yang, Q. Yang, Y. Ma, Z. Xue, J. W. Kwak, T. Jin, Q. Tu, E. Song, Z. Tian, Y. Mei, D. Fang, H. Zhang, Y. Huang, Y. Zhang, J. A. Rogers, *Sci. Robot* **2022**, *7*, eabn0602.
[12] J. Li, P. Angsantikul, W. Liu, B. Esteban-Fernández de vila, S. Thamphiwatana, M. Xu, E. Sandraz, X. Wang, J. Delezuk, W. Gao, L. Zhang, J. Wang, *Angew Chem., Int. Ed.* **2017**, *56*, 2156.
[13] V. Magdanz, I. S. M. Khalil, J. Simmchen, G. P. Furtado, S. Mohanty, J. Gebauer, H. Xu, A. Klingner, A. Aziz, M. Medina-Sánchez, O. G. Schmidt, S. Misra, *Sci. Adv.* **2020**, *6*, eaba5855.
[14] J. Cui, T.-Y. Huang, Z. Luo, P. Testa, H. Gu, X.-Z. Chen, B. J. Nelson, L. J. Heyderman, *Nature* **2019**, *575*, 164.
[15] Q. Wang, Q. Wang, Z. Ning, K. F. Chan, J. Jiang, Y. Wang, L. Su, S. Jiang, B. Wang, B. Y. M. Ip, H. Ko, T. W. H. Leung, P. W. Y. Chiu, S. C. H. Yu, L. Zhang, *Sci. Robot.* **2024**, *9*, eadh1978.
[16] S. Tottori, L. Zhang, F. Qiu, K. K. Krawczyk, A. Franco-Obregón, B. J. Nelson, *Adv. Mater.* **2012**, *24*, 811.
[17] W. Hu, G. Z. Lum, M. Mastrangeli, M. Sitti, *Nature* **2018**, *554*, 81.
[18] H. Zhang, Z. Li, C. Gao, X. Fan, Y. Pang, T. Li, Z. Wu, H. Xie, Q. He, *Sci. Robot.* **2021**, *6*, eaaz9519.
[19] W. Gao, S. Sattayasamitsathit, K. M. Manesh, D. Weihs, J. Wang, *J. Am. Chem. Soc.* **2010**, *132*, 14403.
[20] K. Melde, A. G. Mark, T. Qiu, P. Fischer, *Nature* **2016**, *537*, 518.
[21] Z. Ma, K. Melde, A. G. Athanassiadis, M. Schau, H. Richter, T. Qiu, P. Fischer, *Nat. Commun.* **2020**, *11*, 4537.
[22] W. Wang, S. Li, L. Mair, S. Ahmed, T. J. Huang, T. E. Mallouk, *Angew Chem., Int. Ed.* **2014**, *53*, 3201.
[23] Y. Deng, A. Paskert, Z. Zhang, R. Wittkowski, D. Ahmed, *Sci. Adv.* **2023**, *9*, eadh5260.
[24] J. Durrer, P. Agrawal, A. Ozgul, S. C. F. Neuhauss, N. Nama, D. Ahmed, *Nat. Commun.* **2022**, *13*, 6370.
[25] J. Li, C. C. Mayorga-Martinez, C. Ohl, M. Pumera, *Adv. Funct. Mater.* **2022**, *32*, 2102265.
[26] W. Wang, Q. Liu, I. Tanasijevic, M. F. Reynolds, A. J. Cortese, M. Z. Miskin, M. C. Cao, D. A. Muller, A. C. Molnar, E. Lauga, P. L. McEuen, I. Cohen, *Nature* **2022**, *605*, 681.
[27] H. Li, D. Teal, Z. Liang, H. Kwon, D. Huo, A. Jin, P. Fischer, D. L. Fan, *Nat. Nanotechnol.* **2023**, *18*, 1213.
[28] K. Kim, X. Xu, J. Guo, D. L. Fan, *Nat. Commun.* **2014**, *5*, 3632.
[29] Y. Jin, W. Xu, H. Zhang, R. Li, J. Sun, S. Yang, M. Liu, H. Mao, Z. Wang, *Proc. Natl. Acad. Sci. U.S.A.* **2022**, *119*, e2105459119.
[30] Y. Cao, Y. Huang, J. Zheng, J. Chen, B. Zeng, X. Cheng, C. Wu, J. Wang, J. Tang, *J. Am. Chem. Soc.* **2024**, *146*, 17931.
[31] X. Wu, R. Ehehalt, G. Razinskas, T. Feichtner, J. Qin, B. Hecht, *Nat. Nanotechnol.* **2022**, *17*, 477.
[32] H. Xu, S. Wu, Y. Liu, X. Wang, A. K. Efremov, L. Wang, J. S. McCaskill, M. Medina-Sánchez, O. G. Schmidt, *Nat. Nanotechnol.* **2024**, *19*, 494.
[33] A. Bunea, J. Glückstad, *Laser & Photonics Rev* **2019**, *13*, 1800227.
[34] J. Chen, J. Zhou, Y. Peng, X. Dai, Y. Tan, Y. Zhong, T. Li, Y. Zou, R. Hu, X. Cui, H. P. Ho, B. Z. Gao, H. Zhang, Y. Chen, M. Wang, X. Zhang, J. Qu, Y. Shao, *Adv. Mater.* **2024**, *36*, 2309143.
[35] L. Lin, M. Wang, X. Peng, E N. Lissek, Z. Mao, L. Scarabelli, E. Adkins, S. Coskun, H. E. Unalan, B A. Korgel, L M. Liz-Marzán, E.-L. Florin, Y. Zheng, *Nat. Photon.* **2018**, *12*, 195.
[36] A. Ashkin, J. M. Dziedzic, J. E. Bjorkholm, S. Chu, *Opt. Lett.* **1986**, *11*, 288.
[37] D. G. Grier, *Nature* **2003**, *424*, 810.
[38] K. Dholakia, T. Čižmár, *Nat. Photon.* **2011**, *5*, 335.
[39] J. Gieseler, J. R. Gomez-Solano, A. Magazzù, I. Pérez Castillo, L. Pérez García, M. Gironella-Torrent, X. Viader-Godoy, F. Ritort, G. Pesce, A. V. Arzola, K. Volke-Sepúlveda, G. Volpe, *Adv. Opt. Photon.* **2021**, *13*, 74.
[40] H. Xin, Y. Li, Y. Liu, Y. Zhang, Y. Xiao, B. Li, *Adv. Mater.* **2020**, *32*, 2001994.
[41] U. G. Būtaitė, G. M. Gibson, Y.-L. D. Ho, M. Taverne, J. M. Taylor, D. B. Phillips, *Nat. Commun.* **2019**, *10*, 1215.
[42] J. Leach, H. Mushfique, R. Di Leonardo, M. Padgett, J. Cooper, *Lab Chip* **2006**, *6*, 735.
[43] T. Wu, T. A. Nieminen, S. Mohanty, J. Miotke, R. L. Meyer, H. Rubinsztein-Dunlop, M. W. Berns, *Nat. Photon.* **2012**, *6*, 62.
[44] D. B. Phillips, M. J. Padgett, S. Hanna, Y.-L. D. Ho, D. M. Carberry, M. J. Miles, S. H. Simpson, *Nat. Photon.* **2014**, *8*, 400.
[45] D. B. Phillips, G. M. Gibson, R. Bowman, M. J. Padgett, S. Hanna, D. M. Carberry, M. J. Miles, S. H. Simpson, *Opt. Express.* **2012**, *20*, 29679.
[46] Y. Li, X. Liu, X. Xu, H. Xin, Y. Zhang, B. Li, *Adv. Funct. Mater.* **2019**, *29*, 1905568.
[47] Y. Li, X. Liu, B. Li, *Light Sci. Appl.* **2019**, *8*, 61.
[48] M. J. Villangca, D. Palima, A. R. Bañas, J. Glückstad, *Light Sci. Appl.* **2016**, *5*, e16148.
[49] H. Xin, N. Zhao, Y. Wang, X. Zhao, T. Pan, Y. Shi, B. Li, *Nano Lett.* **2020**, *20*, 7177.
[50] X. Zou, Q. Zheng, D. Wu, H. Lei, *Adv. Funct. Mater.* **2020**, *30*, 2002081.
[51] P. Y. Chiou, A. T. Ohta, M. C. Wu, *Nature* **2005**, *436*, 370.
[52] M. C. Wu, *Nat. Photon.* **2011**, *5*, 322.
[53] S. Zhang, B. Xu, M. Elsayed, F. Nan, W. Liang, J. K. Valley, L. Liu, Q. Huang, M. C. Wu, A. R. Wheeler, *Chem. Soc. Rev.* **2022**, *51*, 9203.
[54] Y. Huang, Z. Liang, M. Alsoraya, J. Guo, D. (Emma) Fan, *Adv. Intell. Syst* **2020**, *2*, 1900127.
[55] Y. Zhang, J. Zhao, H. Yu, P. Li, W. Liang, Z. Liu, G.-B. Lee, L. Liu, W. J. Li, Z. Wang, *Sci. Adv.* **2020**, *6*, eaba9628.
[56] S. Zhang, M. Elsayed, R. Peng, Y. Chen, Y. Zhang, J. Peng, W. Li, M. D. Chamberlain, A. Nikitina, S. Yu, X. Liu, S. L. Neale, A. R. Wheeler, *Nat. Commun.* **2021**, *12*, 5349.
[57] S. Zhang, E. Y. Scott, J. Singh, Y. Chen, Y. Zhang, M. Elsayed, M. D. Chamberlain, N. Shakiba, K. Adams, S. Yu, C. M. Morshead, P. W. Zandstra, A. R. Wheeler, *Proc. Natl. Acad. Sci., U. S. A.* **2019**, *116*, 14823.
[58] L. Mennillo, C. Bendkowski, M. Elsayed, H. Edwards, S. Zhang, V. Pawar, A. R. Wheeler, D. Stoyanov, M. Shaw, *IEEE Robot. Autom. Lett.* **2022**, *7*, 11102.
[59] W. Yang, H. Yu, G. Li, Y. Wang, L. Liu, *Small* **2017**, *13*, 1602769.
[60] X. Hong, B. Xu, G. Li, F. Nan, X. Wang, Q. Liang, W. Dong, W. Dong, H. Sun, Y. Zhang, C. Li, R. Fu, Z. Wang, G. Shen, Y. Wang, Y. Yao, S. Zhang, J. Li, *Sci. Adv.* **2024**, *10*, eadn7582.
[61] J. Frueh, S. Rutkowski, T. Si, M. Gai, C. Gao, S I. Tverdokhlebov, G. Qiu, J. Schmitt, Q. He, Yu-X Ren, J. Wang, *Adv. Photonics Res.* **2022**, *3*, 2100189.
[62] E. Avci, M. Grammatikopoulou, G. Yang, *Adv. Opt. Mater.* **2017**, *5*, 1700031.
[63] J. A. Kim, D. J. Wales, A. J. Thompson, G. Yang, *Adv. Opt. Mater.* **2020**, *8*, 1901934.
[64] S. O'Halloran, A. Pandit, A. Heise, A. Kellett, *Adv. Sci.* **2023**, *10*, 2204072.
[65] X. Wang, X. Chen, C. C. J. Alcântara, S. Sevim, M. Hoop, A. Terzopoulou, C. De Marco, C. Hu, A. J. De Mello, P. Falcaro, S. Furukawa, B. J. Nelson, J. Puigmartí-Luis, S. Pané, *Adv. Mater.* **2019**, *31*, 1901592.
[66] H. Liu, H. Liu, C. Zhu, R. G. Parker, *Mech Mach Theory* **2020**, *145*, 103701.
[67] H. Bay, A. Ess, T. Tuytelaars, L. Van Gool, *CVIU* **2008**, *110*, 346.
[68] R. F. Laine, H. S. Heil, S. Coelho, J. Nixon-Abell, A. Jimenez, T. Wiesner, D. Martínez, T. Galgani, L. Régnier, A. Stubb, G. Follain, S. Webster, J. Goyette, A. Dauphin, A. Salles, S. Culley, G. Jacquemet, B. Hajj, C. Leterrier, R. Henriques, *Nat. Methods* **2023**, *20*, 1949.